Vision-Based Automation Positioning System for Edge-Milling

Hsu Q. Cherng [1], Ngoc V. Ngo [2,*], and Kun M. Chen [1]

[1] Faculty of Mechanical Engineering, National Kaohsiung University of Science and Technology (NKUST), 415 Chien Kung Road, Sanmin District, Kaohsiung 80778, Taiwan, ROC

[2] Faculty of Mechanical Engineering, Thai Nguyen University of Technology (TNUT), No. 666, Street 3-2, Tich Luong Ward, Thai Nguyen, Vietnam

Email: hsuqc@nkust.edu.tw (H.Q.C.); ngocvu@tnut.edu.vn (N.V.N.); s8608012@yahoo.com.tw (K.M.C.)

*Corresponding author

Abstract—**This paper presents the development of a vision-based automated positioning system for machining processes. To achieve accurate positioning and obtain geometric information of machined parts, the relationship between the image coordinate system and the world coordinate system was established through a coordinate calibration process. In this study, a camera was mounted above the working platform to capture images of the machining area. Noise introduced by image subtraction was removed using thresholding operations, followed by edge detection methods to determine the contours of the machined parts. Wind deflectors were used as a case study. A quadratic transformation method was investigated and applied for coordinate calibration. In this process, when the camera resolutions in the OX and OY axes were 0.632 mm/pixel and 0.761 mm/pixel, respectively, the total positioning errors in the OX and OY axes were 1.108 mm and 1.271 mm, respectively. Experimental results demonstrate that the proposed system provides a robust and effective solution for positioning during the machining process.**

Keywords—**image processing, machine vision, positioning system, edge milling**

I. INTRODUCTION

In traditional industries, machines are usually operated and controlled directly by workers. However, with technological advancements, many automation tasks have replaced human operators. In machining processes, different workpieces are typically fixed using jigs and fixtures, which can lead to position deviations. Therefore, a reliable positioning system is essential to address this issue and machine vision-based automatic positioning systems are applied to improve the chamfering process, enhance product quality, and optimize production costs.

In recent years, machine vision systems have been widely applied in manufacturing to enhance both quality and productivity [1–3]. Machine vision integrates illumination, image processing, and analysis to enable non-contact localization, characterization, and manipulation of stationary or moving objects. Features such as size, shape, and color are used to differentiate between acceptable and defective objects [4]. This method is inspired by the human vision system, which detects various types of objects. The acquired information is transmitted to a personal computer via the mainframe computer's signal line, where the spatial positioning of the measured object is calculated within the world coordinate system [5].

Nowadays, machine vision is widely used in quality inspection, non-contact measurement systems, industrial automation, electronic semiconductors, medical applications, defect detection, and more. For instance, Dworkin and Nye [6] developed a machine vision algorithm for measuring hot-formed parts. In their study, CCD cameras were used to capture monochrome and color images under visible light. The images were then acquired, processed through threshold operations, and analyzed. Derganc *et al.* [7] proposed a machine vision system for the automatic measurement of bearing eccentricity. Similarly, Shuxia *et al.* [8] introduced a machine vision-based method to measure the cutting device's diameter and the maximum rotating diameter of a mini-milling machine. Additionally, Hsu *et al.* [9] developed an automatic optical inspection system for detecting and classifying defects in dental floss picks.

Among machine vision applications, the study of Ali *et al.* [10] is very useful for improving precision measurement. The proposed system is to measure gear profile to replace traditional methods which may face danger in measurement process. Besides, the existing methods are either time consuming or expensive. Experimental results of the proposed system were compared with the existing systems. These results showed that their method has great advantages over existing methods in practical application. Rejc *et al.* [11] proposed an automated visual inspection system for dimensional measurements of a protector. A linear and a polynomial approximation were used for defining edges of selected protector structures. Pixel to metric unit transformation was performed by using a higher order polynomial approximation. The measurement accuracy of the proposed system is in the range of ±0.02 mm. The measurement time is less than a second. However,

it cannot replace the current measurement system. It can be only used in the company testing laboratory. Martínez *et al*. [12] presented a quality inspection system for machined metal parts using an image fusion technique. The machine vision system, including one of its main devices, the lighting system performs the detection of flaws on textured surfaces. The proposed system works effectively with a low value of false rejections. An algorithm for automatic inspection of leadframes to detect stamping defects was presented using machine vision [13]. The algorithm used blobs analysis, morphological closing and image subtraction for detecting stamping defects. The proposed system in this study includes a CCD camera, back-lighting source, a computer integrated frame grabber and a conveyor system. The research showed that the system can detect stamping defects on the leadframes a success rate of 98.7%. Machine vision camera systems are typically used for automated inspection of Pressure-Sensitive Paint (PSP) [14]. This research showed relevant imaging characteristics and also showed the applicability of such imaging technology for PSP. The results show that the proposed machine vision system has advanced to such a state that it can now be used for quantitative measurements of a PSP system which can be implemented for under £1000. Zhang *et al*. [15] presented a high precision quality inspection system for steel bars using machine vision. In this study, the Sub-Pixel Boundary Location Method (SPBLM) and Fast Stitch Method (FSM) were proposed. Steel bar diameter, spacing, and quantity were detected. The results show that the proposed system has a high accuracy for calculating diameter and spacing. Lee *et al*. [16] propose an intelligent vision-based Automated Guided Vehicle (AGV) system utilizing fiducial markers. They explore a low-cost and efficient vehicle guidance method using a consumer-grade webcam and fiducial markers. The system employs markers that include a capital letter or a triangle to indicate direction. These markers are easy to produce, manipulate, and maintain. The information encoded in the markers is used to guide the vehicle. Experimental results show that the system achieved a recognition rate of 98.87%.

Vision-based measurement is a promising solution for real-time, non-contact measurement, and numerous studies have focused on this approach for both measurement and object detection. For example, Qia *et al*. [17] proposed an intelligent length measurement method for hot forgings. This work combined sub-pixel edge detection with green laser scanning. First, green laser depth information was used to establish a measurement model. Then, a sub-pixel edge detection algorithm was developed to accurately extract the light bar edge information, enabling the calculation of the forging's length. Finally, the relative positional relationship between the forging and the light bar was analyzed, and an advanced measurement algorithm was presented. In a study by Xiong *et al*. [18], a Canny edge detection algorithm was proposed to address challenges such as image edge noise, poor contrast, and weak edges caused by the complex production environment during the Z-block visual imaging process. This method employed Blob analysis for denoising and Region of Interest (ROI)

positioning, and optimized the gradient strength and direction calculations as well as the local dynamic threshold selection. As a result, high-accuracy edge detection was achieved. In addition, a contour fitting method with sub-pixel accuracy was applied to perform high-precision dimensional measurements. Experimental results showed that the proposed method achieved an average center point positioning error of (5, 5) pixels and an average dimensional measurement error of (0.03, 0.03) mm. An advanced post-processing algorithm was proposed that dynamically modulates detection thresholds based on the distance from the ego object [19]. Their method employed a neural network with self-adaptive thresholding, which significantly reduced false negatives while also decreasing false positives. Experimental results demonstrated that this approach is effective for 3-D object detection and holds promise for applications in field robotics.

Besides, recently advancements in Artificial Intelligence (AI)-based or Machine Learning (ML)-enhanced vision systems have also significantly improved non-contact measurement systems in terms of accuracy, flexibility, and robustness. AI models now could perform precise two-Dimensional (2-D) and three-Dimensional (3-D) measurements from image data, replacing or enhancing traditional rule-based machine vision [20] or deep learning could improve depth and distance estimation from single or stereo images [21].

With the growing demand for industrial automation in the manufacturing sector, machine vision has become increasingly important. In this study, a machine vision system was applied to an automated positioning system during the machining process of wind deflectors. Automation enhances the system's flexibility by adjusting the boundaries of the wind deflectors based on the offset and angular deflection of the machining parts. A camera was used to capture images of three different types of wind deflectors. Prior to image capture, the camera was calibrated to improve accuracy. The captured images were then processed using filtering, thresholding, and other techniques. After obtaining the desired images, the coordinate relationship between the image coordinate system and the world coordinate system was established using the quadratic transformation method. Camera calibration work was also investigated to enhance the accuracy of the calibration process and minimize image distortion, as these factors directly impact the precision of the system.

II. RESEARCH METHODOLOGY

A. Image Processing

In image processing technology for vision-based inspection systems, accurately extracting objects from the initial image is both essential and critical. To effectively isolate the object of interest, it must be separated from the background. In this study, images were captured and then processed using a thresholding operation. The success of thresholding depends on selecting an appropriate threshold value. If the value is set too high, important object details

may be lost and if it is too low, unwanted background elements may remain. Therefore, a suitable threshold value must be determined to eliminate most of the noise while preserving the object of interest. In this work, the threshold value is predefined by the user through a menu in a custom-developed program. This method enables the extraction of relevant image data for subsequent processing.

This study used a Logitech C525 CMOS camera to get image data. The camera was connected to a computer via USB. The camera specifications are shown in Table I.

TABLE I. SPECIFICATIONS OF C525 CMOS CAMERA

No.	Specifications
1	HD video calling (1280×720 pixels) with recommended system
2	HD video capture: Up to 1280×720 pixels
3	Logitech Fluid Crystal™ Technology
4	Autofocus
5	Photos: Up to 8 megapixels
6	Hi-Speed USB 2.0 certified

B. Background Image and Edge Detection

In this work, background subtraction techniques are employed as an effective method for distinguishing foreground objects from the background [22]. This approach is widely used for detecting moving objects. First, a background model is established. Then, the foreground is extracted to identify the target object. Finally, the desired image is generated, as shown in Fig. 1.

Fig. 1 illustrates the presence of noise that must be removed. To address this issue, a thresholding operation was applied to eliminate most of the noise. The threshold value was determined through image subtraction. In this study, to define an appropriate threshold range for extracting the foreground object, only threshold values with more than 20 occurrences were considered, and reference points appearing more than 100 times were used. Based on this analysis, a minimum threshold value of 106 and a maximum of 129 were selected. This process preserves the shape of the wind deflectors while removing extraneous information from the image, as shown in Fig. 2.

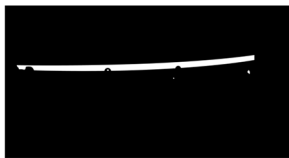Fig. 1. Image subtraction.

Fig. 2. Binarized image.

If the threshold value is set too high, parts of the workpiece image may be lost; conversely, if it is set too low, irrelevant scene details may not be adequately filtered out. To further enhance boundary detection, the Canny algorithm was applied. This algorithm is widely used for edge detection due to its simplicity and robustness. It is based on three key criteria: a low error rate, good localization, and a single response per edge [23]. Using this method, the detected edges closely align with the actual object boundaries, as shown in Fig. 3.
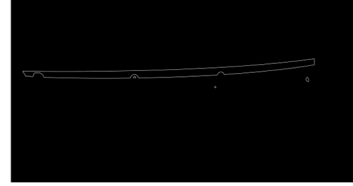

Fig. 3. Canny edge detection.

C. Determining Types of Wind Deflectors

Three types of wind deflectors were used in this study. To classify each type, key geometric properties perimeter, area, and compactness were calculated based on the object's boundary. Compactness is an intrinsic property of an object and is invariant to geometric transformations such as translation, rotation, and scaling. Bribiesca [24] introduced a method for calculating the shape ratio of an object using its perimeter and area to characterize the geometry of machined parts. Following this approach, the compactness of each 2-D object in this study was measured using the following ratio:

$$C = \frac{P^2}{4\pi A} \tag{1}$$

where C denotes compactness, P is the perimeter, and A is the area of the object.

This approach ensures accurate classification of wind deflectors, which is essential for automation in machining processes. Based on the boundary of each wind deflectors, the perimeter, area, and compactness were calculated. The experimental results are presented in Tables II–IV, and the error distributions are illustrated in the histograms shown in Figs. 4–6.

Figs. 4–6 show that the total error in the average compactness was highest for type C at 5.92 mm. The total error for type A was 5.8 mm, while type B exhibited the lowest total error at 2.62 mm. By calculating and comparing the compactness values of the three wind deflectors types, they were successfully classified and recognized within the automated positioning system.

TABLE II. PERIMETER (PIXEL) OF TYPES OF WIND DEFLECTORS

Types	Average	Maximum	Minimum	Positive error	Negative error
A	983.69	997.25	979.94	13.56	3.75
B	1094.17	1098.48	1090.82	4.31	3.35
C	1274.76	1276.15	1273.23	1.39	1.53

TABLE III. AREA (PIXEL^2) OF TYPES OF WIND DEFLECTORS

Types	Average	Maximum	Minimum	Positive error	Negative error
A	8462	8588	8414	126	48
B	9821.7	9992	9706	170.3	115.7
C	12,003.3	12,328	11,788	324.67	215.33

TABLE IV. COMPACTNESS OF TYPES OF WIND DEFLECTORS

Types	Average	Maximum	Minimum	Positive error	Negative error
A	114.36	117.99	112.19	3.63	2.17
B	121.9	123.08	120.46	1.18	1.44
C	135.4	137.94	132.02	2.54	3.38
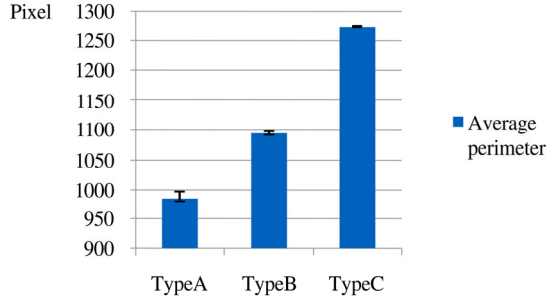
Fig. 4. Average perimeter error.
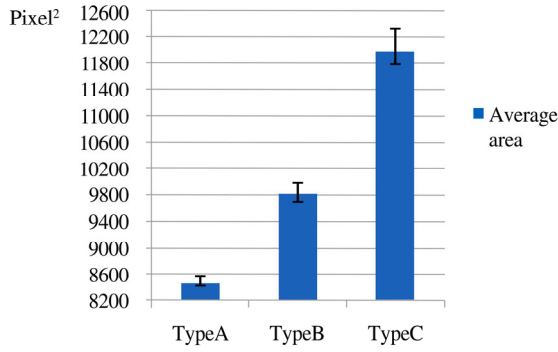
Fig. 5. Average area error.
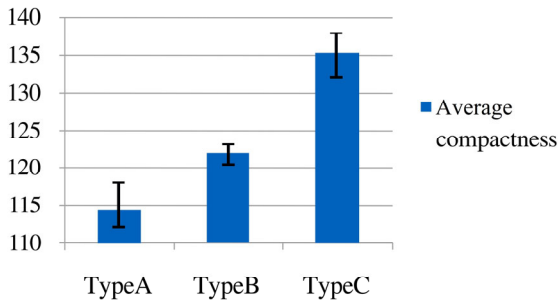
Fig. 6. Average compactness error.

Fig. 7. Schematic of start point and end point.
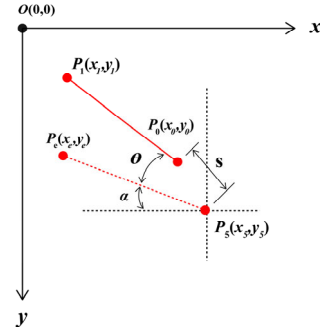
Fig 8. Diagram for calculating the displacement and deflection angle of the wind deflectors.

D. Determining Position of Work-Piece

In Computer Numerical Control (CNC) machining, the boundary limits of the wind deflectors are defined by the positions of its start and end points. Accurate determination of these points is crucial, as they directly influence the precision of the positioning process. These points are identified based on the displacement and angular deflection of the wind deflectors, which are mounted on the same fixture, as illustrated in Figs. 7 and 8.
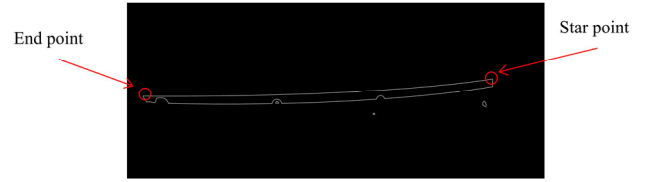
To calculate the displacement and angle deflection of the wind deflectors, a schematic diagram was established, as shown in Fig. 8. Here, O represents the origin of the image coordinate system. $P_s(x_s, y_s)$ and $P_e(x_e, y_e)$ are the initial reference points where displacement and deflection angle are set to zero. $P_0(x_0, y_0)$, $P_1(x_1, y_1)$ represent the start and end points, where displacement and deflection angle are not zero. α denotes the initial angle of the wind deflectors relative to the coordinate system when displacement and deflection angle are zero. S represents the offset, and θ is the angle deflection of the wind deflectors, calculated using Eqs. (2) and (3).

$$S = \sqrt{(x_0 - x_s)^2 + (y_0 - y_s)^2} \qquad (2)$$

$$\theta = sin^{-1}\left[\frac{(x_1 - x_0)(y_e - y_s) - (y_1 - x_0)(x_e - x_s)}{(x_e - x_s)^2 - (y_e - y_s)^2}\right] \qquad (3)$$

E. Coordinate Calibration Method

1) Calibration pattern

In this method, a calibration pattern is used to determine the relationship between the image coordinate system and

the world coordinate system. The calibration pattern contains 910 points, each with a diameter of 10.5 mm. All points are sequentially numbered, and the distance between adjacent points is 19 mm along both the OX and OY axes, as shown in Fig. 9.
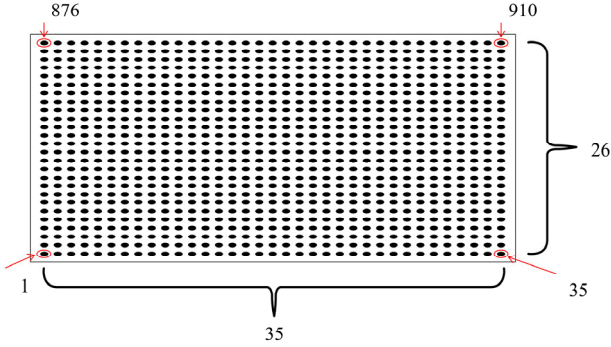
Fig. 9. Size information of the calibration pattern (mm).

2) Quadratic transformation

There are several methods related to coordinate calibration for vision-based inspection systems, such as camera calibration and perspective transformation. However, these methods require the determination of many parameters and are affected by lens distortions, including radial and tangential distortions [25, 26]. Therefore, in this study, quadratic transformation and regression analysis were investigated and applied. This approach establishes the relationship between the image coordinates of point $I(x, y)$ and the world coordinates of point $W(X, Y)$, as described by Eq. (4), and provides sufficient accuracy for the calibration process [27].

$$\begin{cases} X = a_1x^2 + b_1xy + c_1y^2 + e_1x + f_1y + g_1 \\ Y = a_2x^2 + b_2xy + c_2y^2 + e_2x + f_2y + g_2 \end{cases} \quad (4)$$

where a_1, b_1, c_1, e_1, f_1, g_1 and a_2, b_2, c_2, e_2, f_2, g_2 are transformation factors.

To complete the coordinate transformation between the world coordinate system and the image coordinate system, the least squares method is applied, as shown in Eq. (5).

$$\begin{cases} S_X = \sum_{i=1}^{n} \left[X - \left(a_1x_i^2 + b_1x_iy_i + c_1y_i^2 + e_1x_i + f_1y_i + g_1 \right) \right]^2 \\ S_Y = \sum_{i=1}^{n} \left[Y - \left(a_2x_i^2 + b_2x_iy_i + c_2y_i^2 + e_2x_i + f_2y_i + g_2 \right) \right]^2 \end{cases} \quad (5)$$

where S_X and S_Y are summation of the error square with respect to the X and Y coordinate.

With this method, the error analysis results are shown in Figs. 10 and 11. These results indicate that the error in the OX axis ranged from −0.934 mm to 0.590 mm, with a total error of 1.524 mm. In the OY axis, the error ranged from 0.578 mm to 0.797 mm, with a total error of 1.375 mm. The camera resolution was 0.731 mm/pixel and 0.905 mm/pixel in the OX and OY axes, respectively.
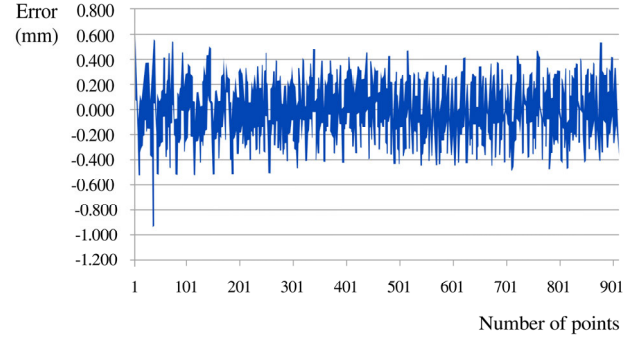
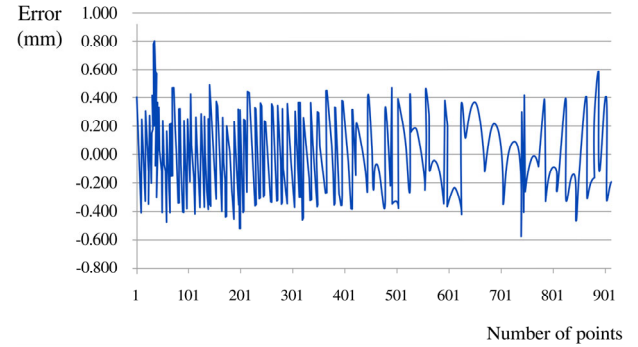Fig. 10. Error in OX axis using regression analysis.

Fig. 11. Error in OY axis using regression analysis.

3) Camera calibration

Calibration accuracy is critical in machine vision because it directly impacts coordinate precision. After completing camera calibration, image coordinates can be accurately transformed into world coordinates. In this work, to test the angle between the camera lens and the work plane, the camera position was fixed in the world coordinate system and rotated to appropriate angles around the OX and OY axes. Subsequently, a binary image was generated, and center points were determined, as shown in Figs. 12 and 13.
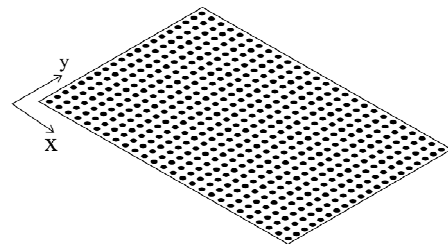
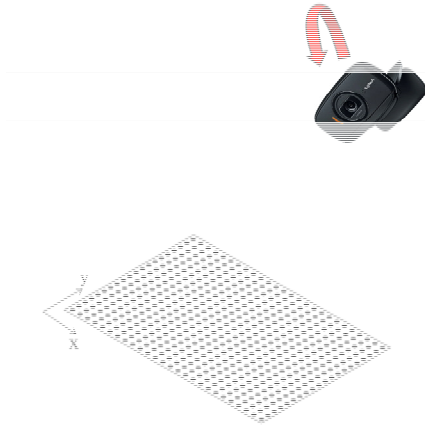Fig. 12. Rotate the camera around OY axis.

Fig. 13. Rotate the camera around OX axis.

Fig. 16. Error in OX axis after rotating camera around OX axis.

Fig. 14 shows that the margin of error was small and stability was maintained before the 600th point; however, after that, the error curve fluctuated irregularly. Fig. 15 illustrates that before the 600th point, the error converged to zero. The error curve changes after rotating the camera around the OY axis of the world coordinate system by a certain angle, as shown in Fig. 12. Subsequently, the coordinates of the center points were determined using a binary image.

Figs. 14–17 show that when the camera was rotated around the OY axis, the error along the OY axis initially decreased to zero but then gradually increased. In contrast, when the camera was rotated around the OX axis, the error curve rose slowly. Different camera angles resulted in varying error levels. The smallest error was observed when the camera was positioned perpendicular to the working platform.
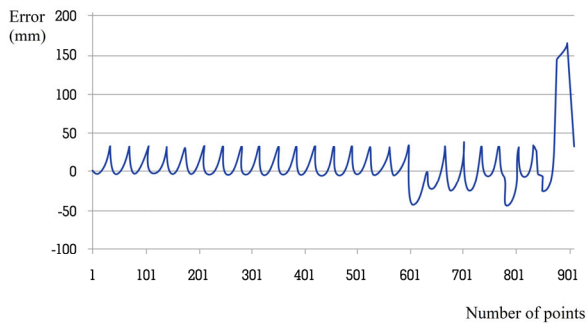

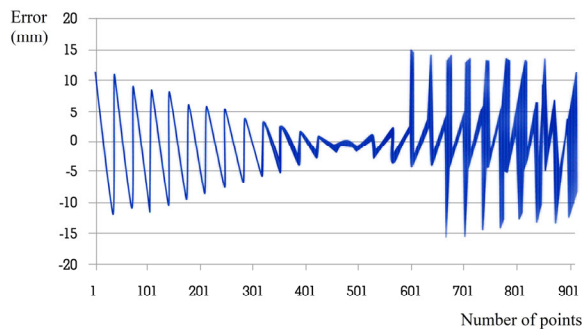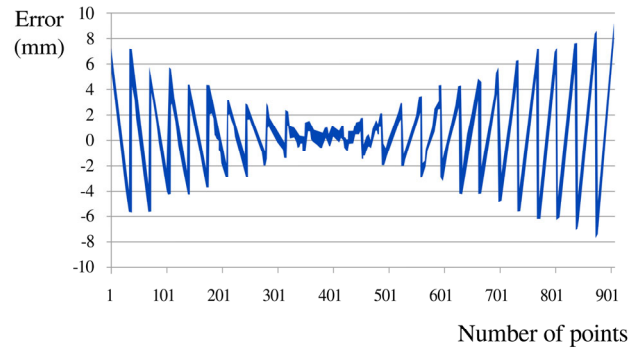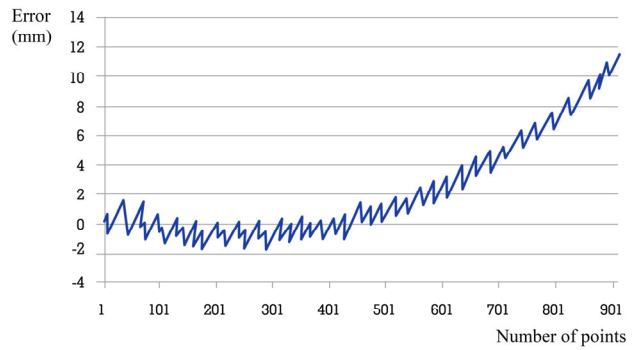Fig. 17. Error in OY axis after rotating camera around OX axis.

The wind deflectors were set up as shown in Fig. 18, where they are located nearly at the center of the image. The error analysis focused on the central area of interest, while other regions indicated in the image were disregarded.

Fig. 14. Error in OX axis after rotating camera around OY axis.

Fig. 18. Image of the wind deflectors.

Figs. 19 and 20 show that, from 315th point to 515th point, the error range in the OX axis was from −0.909 mm to 1.322 mm and the total error was 2.231 mm. In the OY axis, the error ranges from −1.407 mm to 1.408 mm and the total error was 2.815 mm. When compared to the total error over the previous 910 points, these values are significantly smaller. The total error primarily arises from image distortion caused by the camera. Greater deviations correspond to increased distortion. Points near the optical center of the camera exhibit negligible or no distortion; therefore, the workpiece should be positioned at the center of the image to minimize errors.
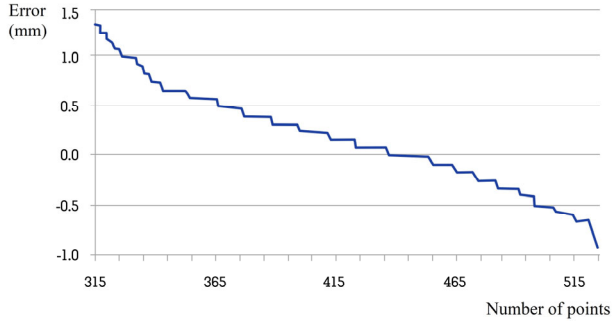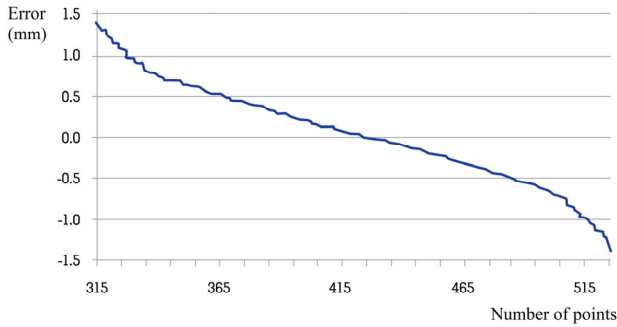

Fig. 15. Error in OY axis after rotating camera around OY axis.

Fig. 19. Error in OX axis.

Fig. 20. Error in OY axis.

III. RESULTS AND DISCUSSION

A. Deflection Angle of the Wind Deflectors

Because the wind deflectors were fixed during the machining process, deflection of the angle was not considered as too large. It was about 2°, 0°, and −2°. So, to check the angle (2°, 0°, −2°), the measurement process was repeated 30 times. Tables V–VII show that when the angle was determined to be 0°, the error value was from 0.574° to −0.572°. The total error was 1.146°. When the angle was 2°, the error value was from 2.572° to −1.281°. The total error was 1.246°. When the angle was −2°, the error value of wind deflector was from −1.573° to −2.738°. The total

error was 1.201°. Experimental results show that when errors were small, they did not significantly affect the accuracy of the positioning system, therefore these errors were within an accepted range.

TABLE V. REPETITION OF 30 TIMES FOR THE DEFLECTION MEASURED VALUE OF ANGLE 0°

Deflection Angle	Values
0° (Unit °)	0.096, 0.574, 0.569, 0.287, −0.093, 0.368, 0.286, 0.570, 0.064, 0.096, 0.177, 0.173, 0.096, −0.082, 0.546, 0.001, −0.370, 0.326, 0.097, −0.176 −0.572, 0.287, −0.569, 0.538, 0.286, 0.569, 0.546, 0.483, −0.013, 0.091

TABLE VI. REPETITION OF 30 TIMES FOR THE DEFLECTION MEASURED VALUE OF ANGLE 2°

Deflection Angle	Values
2° (Unit °)	1.437, 2.013, 2.005, 2.481, 2.188, 2.005, 1.746, 1.381, 1.696, 2.398, 2.387, 1.281, 2.372, 1.329, 1.439, 1.940, 1.955, 1.381, 1.381, 2.527, 2.247, 1.872, 2.501, 1.987, 2.112, 1.478, 2.105, 1.911, 1.842, 1.909

TABLE VII. REPETITION 30 TIMES FOR THE DEFLECTION MEASURED VALUE OF ANGLE −2°

Deflection angle	Values
−2° (Unit °)	−2.015, −2.539, −1.568, −2.704, −2.694, −1.848, −1.937, −2.129, −2.738, −1.688, −1.586, −1.691, −1.673, −2.372, −2.087, −1.562, −1.977, −2.343, −1.682, −1.653, −2.139, −1.537, −2.589, −2.310, −1.832, −1.839, −1.542, −2.178, −2.433, −1.801

B. Improvement of the Image Resolution and Calibration Error

To improve image resolution, the height of the camera was lowered, and the area enclosed by the boundary perimeter was re-measured. Subsequently, the compactness was calculated. The camera resolution was adjusted to 0.632 mm/pixel and 0.761 mm/pixel along the OX and OY axes, respectively. These results are shown in Tables VIII– X.

TABLE VIII. PERIMETER (PIXEL) OF TYPES OF WIND DEFLECTORS

Type	Average	Maximum	Minimum	Positive error	Negative error
A	1063.3	1211	928	147.7	135.3
B	1349.23	1359	1339	9.77	10.23
C	1527.8	1569	1490	41.2	37.8

TABLE IX. AREA (PIXEL^2) OF TYPES OF WIND DEFLECTORS

Type	Average	Maximum	Minimum	Positive error	Negative error
A	10,078.1	13,009	7553	2930.9	2525.1
B	14,864.77	15,157	14,585	292.23	279.77
C	17,495.03	18,521	16,345	1025.97	1150.03

TABLE X. COMPACTNESS OF TYPES OF WIND DEFLECTORS

Type	Average	Maximum	Minimum	Positive error	Negative error
A	113.05	116.42	110.3	3.37	2.75
B	122.47	123.58	121.49	1.11	0.98
C	133.47	136	130.82	2.53	2.56

Tables VIII–X show that Type A, which has the smallest perimeter and area, exhibited the highest total error in

average compactness, with a value of 6.12. Type B had the lowest total error in average compactness, at 2.09, while

Type C's total error was 5.09. The error distributions are illustrated in the histograms shown in Figs. 21–23.
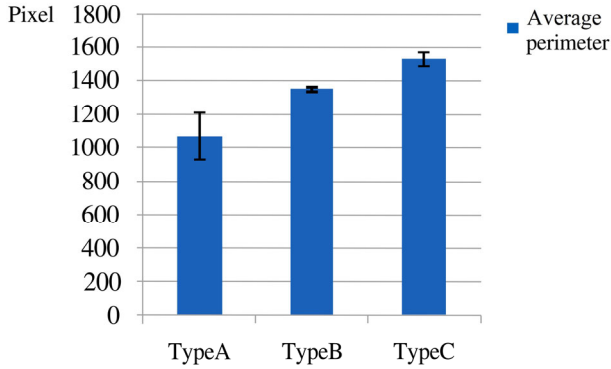

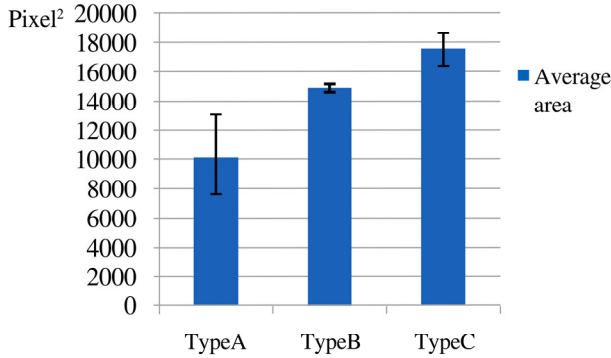Fig. 21. Average perimeter error after raising the resolution.

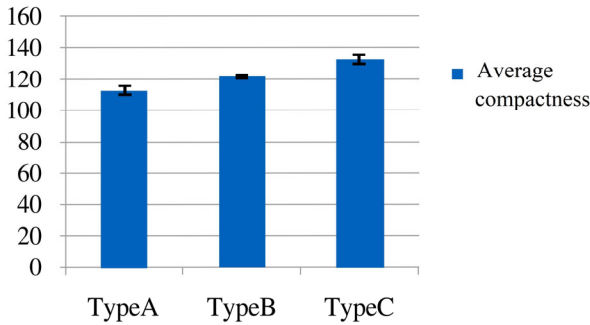Fig. 22. Average area error after raising the resolution.

Fig. 23. Average compactness error after raising the resolution.

Moreover, to reduce coordinate transformation error, 43 calibration points and regression analysis were used to replace the previously determined 910 points. After changing the camera resolution, the error in the OX axis ranged from 0.606 mm to −0.502 mm, resulting in a total error of 1.108 mm, as shown on Fig. 24. Similarly, the error in the OY axis ranged from 0.684 mm to −0.587 mm, with a total error of 1.271 mm, as shown in Fig. 25. The results obtained from the regression analysis showed a significant improvement compared to the previous results, with the total error reduced to 0.416 mm and 0.104 mm in the OX and OY axes, respectively. Therefore, a higher camera resolution led to lower errors.
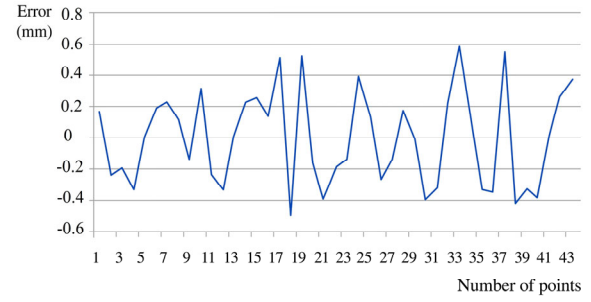

Fig. 24. Error in OX axis after improving the resolution of the regression analysis.
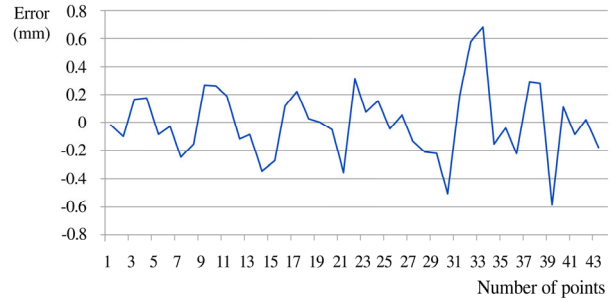

Fig. 25. Error in OY axis after improving the resolution of the regression analysis.

IV. CONCLUSION

In this study, a machine vision-based positioning system for wind deflectors was successfully developed. The key conclusions are as follows:

The background subtraction method proved effective for isolating the wind deflectors from the working platform during image processing.

In calibration work, experimental results showed that the coordinate transformation error increases as the angle between the camera mirror axis and the working platform grows. The error and image distortion are minimized when the camera is located perpendicular to the working platform.

Camera resolution significantly impacts coordinate calibration accuracy. With resolutions of 0.632 mm/pixel and 0.761 mm/pixel in the OX and OY axes, total errors of 1.108 mm and 1.271 mm were observed, respectively.

To further reduce calibration errors, future work will focus on using higher resolution cameras and implementing controlled lighting conditions in the machine vision system to improve image resolution and increase measurement accuracy.

CONFLICT OF INTEREST

The authors declare no conflict of interest.

AUTHOR CONTRIBUTIONS

Hsu Q. Cherng provided conceptual guidance, supervised the research work, and contributed to manuscript revisions. Ngoc V. Ngo analyzed the data, prepared the initial draft, wrote the manuscript, and performed a critical review of the manuscript. Kun M. Chen conducted the experiments, analyzed the data, and

prepared the initial draft. All authors had approved the final version.

REFERENCES

[1] Z. You, H. Gao, L. Guo *et al.*, "Machine vision based adaptive online condition monitoring for milling cutter under spindle rotation," *Mechanical Systems and Signal Processing*, vol. 171, 108904, 2022.

[2] T. Banda, A. A. Farid, C. Li *et al.*, "Application of machine vision for tool condition monitoring and tool performance optimization—A review," *The International Journal of Advanced Manufacturing Technology*, vol. 121, no. 11, pp. 7057–7086, 2022.

[3] J. Qu, , C. Yue, J. Zhou *et al.* "On-machine detection of face milling cutter damage based on machine vision," *The International Journal of Advanced Manufacturing Technology*, vol. 133, no. 3, pp. 1865–1879, 2024.

[4] D. Marr and T. Poggio, "Cooperative computation of stereo disparity," *Science*, vol. 194, pp. 283–287, 1976 .

[5] R. Laganière, *OpenCV 2 Computer Vision Application Programming Cookbook*, Packt Publishing Limited, 2011.

[6] S. B. Dworkin and T. J. Nye, "Image processing for machine vision measurement of hot formed parts," *Journal of Materials Processing Technology*, vol. 174, no. 1–3, pp. 1–6, 2006.

[7] J. Derganc, B. Likar, and F. Pernus, "A machine vision system for measuring the eccentricity of bearings," *Computer in Industrial*, vol. 50, pp. 103–111, 2003.

[8] S. Guo, J. Zhang, X. Jiang, Y. Peng, and L. Wang, "Mini milling cutter measurement based on machine vision," *Procedia Engineering*, vol. 15, pp. 1807–1811, 2011.

[9] Q. C. Hsu, C. W. Lin, and J. Y. Chen, "Development of an automatic optical inspection system for defect detection of dental floss picks," in *Proc. 2012 IEEE/ASME International Conference onAdvanced Intelligent Mechatronics*, 2012, pp. 444–449.

[10] M. H. Ali, S. Kurokawa, and K. Uesugi, "Camera based precision measurement in improving measurement accuracy," *Measurement*, vol. 49, pp. 138–147, 2014.

[11] J. Rejc, F. Kovačič, A. Trpin *et al.*, "The mechanical assembly dimensional measurements with the automated visual inspection system," *Expert Systems with Applications*, vol. 38, no. 8, pp. 10665–10675, 2011.

[12] S. S. Martínez, C. O. Vázquez, J. G. García, and J. G. Ortega, "Quality inspection of machined metal parts using an image fusion technique," *Measurement*, vol. 111, pp. 374–383, 2017.

[13] A. Bhuvanesh and M. R. Mani, "Automatic detection of stamping defects in leadframes using machine vision: Overcoming translational and rotational misalignment," *The International Journal of Advanced Manufacturing Technology*, vol. 32, pp. 1201–1210, 2007.

[14] M. K. Quinn, E. Spinosa, and D. A. Roberts,"Miniaturisation of pressure-sensitive paint measurement systems using low-cost, miniaturised machine vision cameras," *Sensors*, vol. 17, no. 8, p. 1708, 2017.

[15] X. Zhang, J. Zhang, M. Ma *et al.*, "A high precision quality inspection system for steel bars based on machine vision," *Sensors*, vol. 18, no. 8, p. 2732, 2018.

[16] J. Lee, C. H. Hyun, and M. Park, "A vision-based automated guided vehicle system with marker recognition for indoor use," *Sensors*, vol. 13, no. 8, pp. 10052–10073, 2013.

[17] L. Qian, Y. C. Zhang, T. Kong, and Q. Li, "Intelligent length measurement method of hot forgings combining sub-pixel edge detection and green laser scanning," *International Journal of Precision Engineering and Manufacturing*, vol. 26, no. 2, pp. 363–376, 2025.

[18] J. Xiong, D. Wang, J. Yin, and R. Wu, "Precise Z-Block positioning and dimension measurement using improved Canny edge detection and sub-pixel contour fitting," *The Journal of Supercomputing*, vol. 81, no. 1, pp. 1–31, 2025.

[19] H. Liu, C. Wang, X. Zhan *et al.*, "Enhancing 3D object detection by using neural network with self-adaptive thresholding," arXiv Preprint, arXiv:2405.07479, 2024.

[20] S. Mehrishal, J. Kim, Y. Shao, and J. J. Song, "Artificial intelligence-aided semi-automatic joint trace detection from textured three-dimensional models of rock mass," *Journal of Rock Mechanics and Geotechnical Engineering*, vol. 17, no. 4, pp. 1973–1985, 2025.

[21] M. Zürn, C. Schmerbeck, A. Kernbach *et al.*, "Robotic wiring harness bin picking solution using a deep-learning-based spline prediction and a multi-stereo camera setup," in *Proc. Stuttgart Conference on Automotive Production*, 2025, pp. 319–334.

[22] L. Li, W. Huang, I. Y. H. Gu, and Q. Tian, "Foreground object detection in changing background based on color co-occurrence statistics," *Sixth IEEE Workshop on Applications of Computer Vision*, pp. 269–274, 2002.

[23] R. C. Gonzalez and R. E. Woods, *Digital Image Processing*, 3rd ed. Pearson Education Taiwan Ltd., 2008.

[24] E. Bribiesca, "A measure of compactness for 3D shapes," *Computers & Mathematics with Applications*, vol. 40, no. 10–11, pp. 1275–1284, 2000.

[25] J. Yu, N. Gao, Z. Meng, and Z. Zhang, "High-accuracy projector calibration method for fringe projection profilometry considering perspective transformation," *Optics Express*, vol. 29, no. 10, pp. 15053–15066, 2021.

[26] J. Yu, Y. Liu, Z. Zhang *et al.*, "High-accuracy camera calibration method based on coded concentric ring center extraction," *Optics Express*, vol. 30, no. 23, pp. 42454–42469, 2022.

[27] Q. C. Hsu, N. V. Ngo, and R. H. Ni, "Development of a faster classification system for metal parts using machine vision under different lighting environments," *The International Journal of Advanced Manufacturing Technology*, vol. 100, no. 9, pp. 3219–3235, 2019.